Journal of Catalysis **207,** 127–138 (2002)
doi:10.1006/jcat.2002.3512, available online at http://www.idealibrary.com on IDEAL®

Trichloroethene Dechlorination Reactions on the PdCu(110) Alloy Surface: A Periodical Density Functional Theory Study of the Mechanism

L. A. M. M. Barbosa*,†,[1,2] and P. Sautet*,†

*Institut de Recherches sur la Catalyse, Centre National de la Recherche Scientifique, 2 Avenue Albert Einstein, Villeurbanne Cedex 69626, France; and †Laboratoire de Chimie Théorique et des Matériaux Hybrides, Ecole Normale Supérieure de Lyon, 46, Allée d'Italie, Lyon 69364 Cedex 07, France

Received October 17, 2001; revised January 10, 2002; accepted January 12, 2002

In the present work the dissociation of the trichloroethene on the PdCu(110) surface has been investigated by applying *ab initio* periodic density functional theory. The reaction steps, intermediates and transition states of this reaction have been identified. Two different mechanisms have been studied, starting from the most stable adsorption modes of trichloroethene (di-σ structures). Regarding the reaction path, all intermediate steps are exothermic. In addition, all activation energies are relatively small (<40 kJ mol^{-1}). Therefore, this reaction is shown to be kinetically and thermodynamically favorable on this surface. From the intermediate steps of both mechanisms, it was possible to attain additional information about dechlorination reactions, for the other chloroethene molecules (dichloro and chloro). There is good evidence that the intermediates and transition states for the dechlorination reaction of these molecules have a similar configuration on the PdCu surface. A detailed study of the transition states indicated that the activation energy of the dissociation step increases with the rebonding energy of chlorine on the surface, which is a common fragment to all different transition states. This also confirms that these transition state are "early" ones. A simple kinetic model has been constructed with the elementary step rate constants evaluated from the calculations. The reactional system has been shown to be very complex. Most of all intermediates are present on the surface simultaneously, in accordance with experimental studies.

1. INTRODUCTION

The reduction of the amount of chlorohydrocarbons and chlorofluorhydrocarbons, which are deeply related to the problems of the ozone layer destruction and groundwater contamination, has become an important environmental demand.

The search for catalysts able to dissociate the carbon–halogen bond is strongly desired and necessary. In addition, understanding this carbon-halogen bond dissociation is a key step toward modifying and increasing the activity and selectivity of the catalyst for this reaction.

The cleavage of the C–Cl bond has been exhaustively studied in the past few years. Metals such as Pt, Pd, and Cu have been suggested to be excellent catalysts for the dechlorination reaction (1–20). On Cu surfaces, the dissociation of saturated alkyl halides depends on the size of the alkyl chain (19), as small alkyl halides desorb without dissociation.

On the other hand the C–Cl bond dissociation becomes facile with an increase in the number of chlorine atoms in the molecule, with it being easier in the CCl_2 group than the CCl one (13). The second C–Cl bond cleavage is easier than the initial one and is dominated by β-chlorine elimination (13).

These results have been also noted for the dissociation of dichlorofluoroethanes (with different fluorine content) on Pd(111) (7, 10). The rate constant for this reaction increases if the CCl_2 group is considered. Furthermore, the electronic distribution of the transition state for the C–Cl bond cleavage has been suggested to be very similar to the initial state (6). The intrinsic activation energy for C–Cl cleavage has been estimated to be around 65–70 kJ mol^{-1}.

On supported Pd catalysts (21, 22) the same behavior is observed for these multiply chlorinated fluoroethanes, which react in higher turnover rates than the monochlorinated molecules.

Multiply chlorinated ethenes have been also shown to dissociate promptly on Cu surfaces. The addition of chlorine atoms to the ethene molecule seems to decrease the rate of desorption (14), increasing the dissociation. In the case of dichloroethenes (*cis* and *trans*), the major product is found to be acetylene at 200 K and benzene at 300 K (12), whereas for the 1,1-dichloro-isomer the major product is 1,3-butadiene (23). By adding one more chlorine to the molecule (trichloroethene), only acetylene and carbon deposits have been noticed on the Cu surface at 300 K (9). Above this temperature there is competition between the

[1] Present address: ICI Strategic Technology group, Wilton Centre, Middlesbrough, U.K. Fax: +44 1642 436200. E-mail: luis.barbosa@ici.com.
[2] To whom correspondence should be addressed.

0021-9517/02 $35.00

desorption of the acetylene and the trimerization reaction, which forms benzene.

Recently the dissociation of trichloroethene (TCE) on a PdCu(110) surface has been studied by comparing the experimental (high-resolution electron energy loss spectroscopy (HREELS)) and the calculated vibrational frequencies of the intermediate species (24). Surface reactions occur relatively early (200 K) and most of the CCl bonds have been already broken at 280 K. Between 200 and 280 K, the di-σ chemisorbed species, as well as the first and second dechlorination products (dichloro and monochloro species) are present on the surface simultaneously in different concentrations. It was not possible to monitor the sequential cleavage of the three C–Cl bonds, which indicates the complexity of this process.

In order to obtain better insight into the mechanism and different pathways of this dechlorination reaction, periodical quantum chemical calculations have been employed here. The analysis, at a molecular level, of this reaction offers an opportunity to also investigate the dechlorination mechanism of parent molecules: the dichloroethenes (*cis*, *trans*, and 1,1-isomers). Moreover, trichloroethene has two different functional groups, CHCl and CCl_2, which provides additional information about the effect of the number of chlorine atoms on the kinetics of the C–Cl bond cleavage.

2. METHODS

All geometry optimizations and transition state searches were performed using the Vienna Ab-initio Simulation Package (VASP) (25, 26). This code carries out periodic density functional calculations (DFT) using pseudopotentials and a plane-wave basis set. The DFT was parameterized in the local-density approximation (LDA), using the exchange-correlation functional proposed by Perdew and Zunger (27) and corrected for nonlocality in the generalized gradient approximations (GGA) using the Perdew–Wang 91 functional (28). The interaction between the core and electrons is described using the ultrasoft pseudopotentials introduced by Vanderbilt (29) and provided by Kresse and Hafner (30).

The PdCu(110) surface is usually cleaned and stabilized by annealing at high temperature (24). After this procedure a well-defined Cu-rich surface is formed with a mean copper concentration in the top layer of 70%, instead of 50% in the bulk. Furthermore, low-energy electron diffraction (LEED) and scanning tunneling microscope (STM) show a well-ordered (2 × 1) structure, with all the results being characteristic of the formation of a α'-Cu_3Pd phase, with alternation of pure Cu and mixed PdCu planes (31).

A slab with an ordered $PdCu_3$(110) structure can be considered a good model for the surface region of the $Pd_{50}Cu_{50}$ alloy. The first layer of this model is formed by an equal number of Pd/Cu atoms and the second layer is composed of only Cu atoms. Then a periodic five-layer slab is constructed alternating these two layers (Fig. 1), yielding surface Pd atoms surrounded by Cu atoms and a copper concentration of about 70% (32).

Trichloroethene is only adsorbed on one side of the slab. One slab is separated from its periodic image in the z direction by a vacuum space which is equivalent to five metallic layers. Each layer is composed of eight metallic atoms and only the bottom layer is maintained frozen in all optimizations.

In order to minimize the effect of the stress that occurs due to the constraints in the slab model, the optimal bulk metal–metal distance was calculated. The calculated bulk nearest Pd–Cu distance is 2.70 Å, which is in good agreement with the measured value of 2.62 Å for the $PdCu_3$ alloy (33).

In the slab model trichloroethene is ordered over the surface in the following structure: (4 × 2) 0.125 ML. The different intermediates are also optimized with the same original unit-cell; however local coverage increases due to the presence of chlorine atoms, which are produced from the dechlorination reaction.

The search for the transition state is done by following the reaction coordinate. Different points of the reaction path are obtained by displacing both C and Cl atoms of the C–Cl bond, fixing their spatial positions and optimizing the resulted system. Once found, the stationary point, which corresponds to the configuration with the maximum energy in this path, is reoptimized without the previous constraints. This optimization is done by minimizing the forces on the atoms of the system with the quasi-Newton algorithm, as implemented in VASP. The structure is considered to be converged when these forces become smaller than 0.01 eV $Å^{-1}$.

All stationary points are checked by frequency calculations. Transition states (Ts) are characterized by the appearance of one imaginary frequency (34). All imaginary frequencies with values <10 cm^{-1} are considered negligible within the accuracy of the method and discarded. More details about the frequency calculations which have been employed here can be found elsewhere (24).

For each dissociation step on the surface the rate constant k_{diss} at a temperature T is evaluated using (35).

$$k_{diss} = \frac{k_B T}{h} \frac{pf^{Ts}}{pf^{Rs}} \exp\left(-\frac{E_a}{RT}\right), \qquad [1]$$

where k_B is Boltzmann's constant, h is Planck's constant, R is the gas constant, and E_a is the activation energy per mole between the reactants and the transition state, corrected for the zero-point energy vibrations (ZPE). pf^{Rs} and pf^{Ts} are partition functions at the reactant and the transition

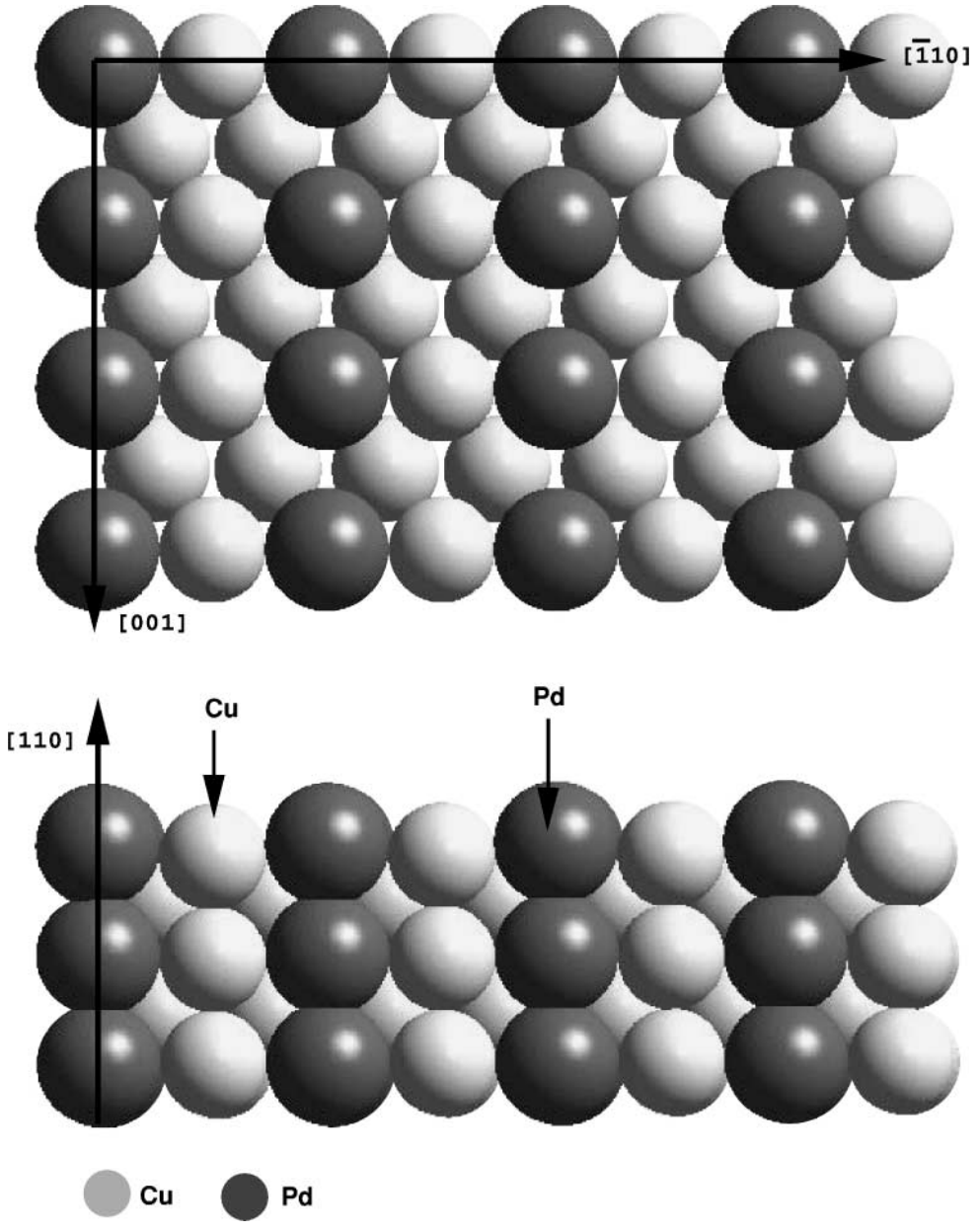

FIG. 1. Surface model of PdCu(110) used in all calculations.

state, respectively. In the present case, the surface is assumed to be rigid; therefore its partition functions are equal to the unity and do not appear in the calculation of the kinetic constant. Both the reactant and transition state are localized on the surface; thus there is no rotation or translation motion but only various vibration modes. The vibrational partition functions at the reactant and the transition state are evaluated using

$$pf = \prod_i \frac{\exp\left(+\frac{1}{2}\frac{h\nu_i}{k_B T}\right)}{1 - \exp\left(-\frac{h\nu_i}{k_B T}\right)}. \qquad [2]$$

The Brillouin-zone integrations are performed on a $2 \times 3 \times 1$ Monkhorst-Pack grid of K-points for all structures, which allows convergence for the calculated energy to be reached. The ZPE correction is only applied for the evaluation of the rate constants. All values for the activation and reaction energies, shown in all schemes, are not corrected for ZPE. A spin restricted approach is used, since spin polarization effects have been found to be negligible in other works using Pd surfaces (36–38). The only exception was made for the case of calculations of the chlorine and molecular radicals in the study of the rebonding energy of such fragments on the surface.

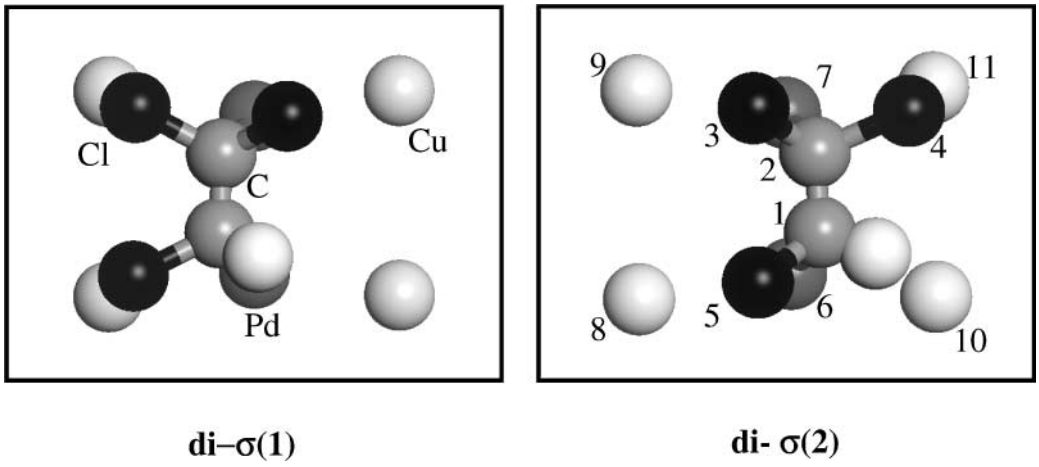

FIG. 2. Initial configuration of the di-σ species on the PdCu surface. Cu, Pd, and Cl atoms are shown by light grey, dark gray, and black spheres, respectively. Only the upper layer of the surface is shown in all figures.

3. RESULTS

Previously, different adsorption modes of TCE have been analyzed on the PdCu(110) surface, which correspond to three different families: bridge, top, and hollow (32). In the first mode mainly the carbon atoms interact with the surface, whereas in the last one the chlorine atoms play the major role. At the top position, both carbon and chlorine atoms can interact preferentially with the surface. The most stable configurations of the trichloroethene correspond to the di-σ species (Fig. 2) due to the combination of two interactions with the surface: Pd–C and Cl–Cu, which are formed on adsorption of the molecule.

For one configuration (di-$\sigma(1)$), besides the main Pd–C bonds, two chlorine atoms interact with the surface, whereas in the other configuration (di-$\sigma(2)$) only one chlorine atom interacts. Labels 1 and 2 are related to relative stability, with 1 being the most stable di-σ configuration.

First Dissociation Step

In this step two different pathways are investigated for the C–Cl bond dissociation. The main difference is the functional group from which the Cl atom leaves: CCl_2 and CHCl. Previously, it was shown that the C–Cl(4) bond of the configuration di-$\sigma(2)$ and the C–Cl(5) bond of the other di-σ structure have strong elongation (32). These two activated C–Cl bonds are selected as starting points for the dissociation reaction. Scheme 1 reports the dissociation path for the for C–Cl(5) (di-$\sigma(1)$) and Scheme 2 for C–Cl (4) (di-$\sigma(2)$).

Barriers for the first C–Cl cleavage are small and the reaction is strongly exothermic. One may note that the C–Cl bond from the CCl_2 group cleaves with the lowest activation energy, 8 kJ mol^{-1}. The large value for the reaction energy suggests that both processes have an early transition state, which is confirmed by the similarities between the transition state and the chemisorbed species (see Tables 1 and 2). For instance the C–Cl bond is only weakly elongated in both transition states.

TABLE 1

Calculated Distance for All Species Formed in the Dissociation Path Starting with the di-$\sigma(1)$ Structure on the PdCu Surface

	Species						
Bond	di-$\sigma(1)$	Ts1	diCl(1)	Ts2	MonoCl(1)	Ts3	CCH(1)
d(1–2)	1.47	1.43	1.38	1.34	1.38	1.37	1.33
d(1–5)	1.83	2.25	4.64	4.65	5.42	5.44	5.34
d(1–6)	2.09	2.02	2.07	2.09	2.09	2.10	2.14
d(2–3)	1.82	1.82	1.81	2.28	3.77	3.82	3.87
d(2–4)	1.79	1.79	1.76	1.71	1.81	2.04	3.46
d(2–7)	2.07	2.11	2.25	2.10	2.10	2.05	2.02
d(3–9)	2.47	2.34	2.41	2.22	2.21	2.22	2.23
d(4–11)	4.02	4.51	4.63	4.63	2.85	2.41	2.29
d(5–8)	2.44	2.32	2.27	2.25	2.25	2.25	2.23

Note. Values in Å. The atom numbers are shown in Fig. 2.

TABLE 2

Calculated Distance for All Species Formed in the Dissociation Path Starting with the di-$\sigma(2)$ Structure on the PdCu Surface

	Species						
Bond	di-$\sigma(2)$	Ts1	diCl(2)	Ts2	MonoCl(2)	Ts3	CCH(2)
d(1–2)	1.46	1.45	1.38	1.37	1.35	1.28	1.31
d(1–5)	1.77	1.77	1.74	1.72	1.77	2.37	3.67
d(1–6)	2.12	2.13	2.46	2.55	2.83	2.79	3.16
d(2–3)	1.76	1.74	1.82	2.50	5.08	5.00	4.44
d(2–4)	1.89	2.15	4.51	4.23	3.83	3.92	4.52
d(2–7)	2.07	2.02	2.08	2.00	2.10	2.15	2.68
d(3–8)	5.32	5.31	2.60	2.24	2.24	2.23	2.23
d(4–11)	2.43	2.31	2.25	2.25	2.28	2.27	2.29
d(5–6)	2.98	3.04	3.68	3.70	2.85	2.48	2.54

Note. Values in Å. The atom numbers are shown in Fig. 2.

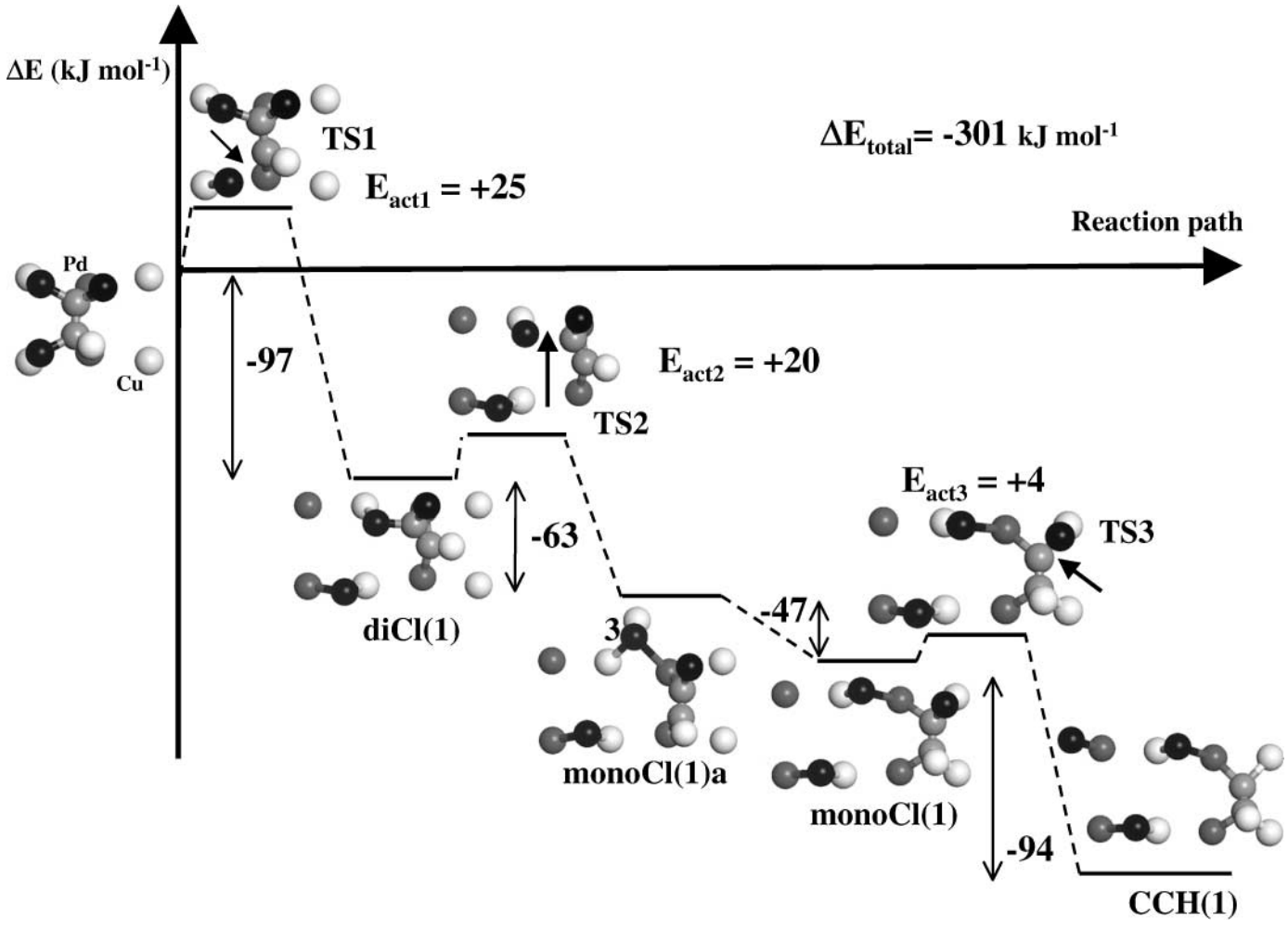

SCHEME 1. Dechlorination reaction path for the di-σ(1) configuration. The three successive reaction steps are shown, with the transition states (Ts) and intermediates. The arrows represent, for each step, the C–Cl bond which is being cleaved. The atoms are Cl (black), Pd (dark grey), C (grey), Cu (light grey), and H (white).

It is interesting to observe that these results are in accordance with the Brønsted–Evans–Polanyi relation: TCE under the di-σ(2) configuration on the PdCu surface has the largest reaction energy, thus the lowest activation energy to dissociate.

Experimentally, the dissociation of the chlorine bond from multiply chlorinated molecules has been suggested to be more favorable on Pd (10) and Cu surfaces (13, 14). Moreover, for the case of chloro fluorocarbons (6, 7), it has been suggested that the dissociation of C–Cl bond has "early" transition states. These points are in a good agreement with the results shown here.

The products formed in both first-dissociation mechanisms (diCl(1) and diCl(2)) are very similar. On C–Cl bond dissociation, these molecules move toward the surface. A vinyl type species is formed with a strong σ bond (C–Pd). There is an additional interaction of the π orbital of the C–C bond with the neighboring Pd atom, as shown in Schemes 1 and 2. This interaction is also indicated by the change in the C–Pd distance in the di-σ and diCl species (see d(2–7) and d(1–6) in Tables 1 and 2, respectively). These C–Pd distances for the case of the diCl species are, however, larger than the calculated value for the π chemisorption mode of trichloroethene (2.17 Å) (32).

This first dissociation, shown in Scheme 1, can be considered a model for the dehalogenation reaction of vinyl halides; the main product will have a similar molecular structure and spatial configuration. Bent and coworkers. (16) studied the dissociation of vinyl halides on Cu(110). They observed that the C–Br bond cleavage occurs at 160 and at 250 K. The vinyl fragments on the surface coupled to yield 1,3-butadiene with 100% selectivity. Both experimental findings are in good agreement with the results found here. The activation energy found for the C–Cl bond of the CHCl group has a small value, 25 kJ mol^{-1}, which explains the low temperature for dissociation. Moreover, the coupling of two vinyl intermediates, having the structure proposed here, can produce 1,3-butadiene in a selective way.

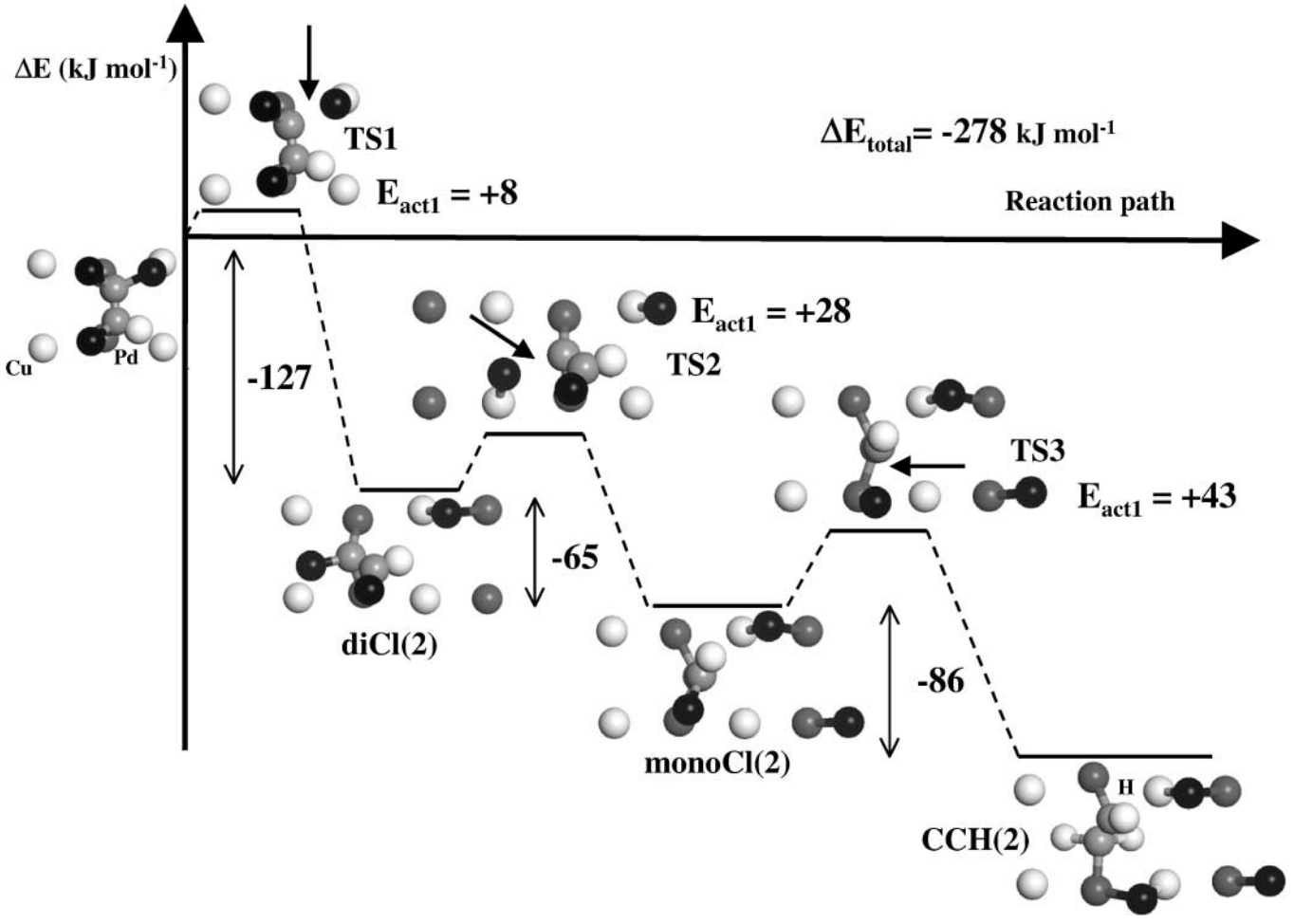

SCHEME 2. Dechlorination reaction path for the di-$\sigma(2)$ configuration. The three successive reaction steps are shown, with the transition states (Ts) and intermediates. The arrows represent, for each step, the C–Cl bond which is being cleaved. The atoms are Cl (black), Pd (dark grey), C (grey), Cu (light grey), and H (white).

Second Dissociation Step

The second dissociation starts from the previous diCl configurations. The C–Cl bond of the CCl_2 group is again the most favorable for dissociation (see Scheme 1). The activation barrier for this C–Cl bond is, however, only slightly smaller (20 kJ mol^{-1}) than the one for the CCl group (28 kJ mol^{-1}) (see Scheme 2). The lowest value of the activation energy found for the first step of the di-$\sigma(2)$ configuration (8 kJ mol^{-1}) is due to the stronger activation of the C–Cl bond. This can be seen by the C–Cl bond lengths of the diCl(1) (1.81 Å) and di-$\sigma(2)$ (1.89 Å) structures (see Table 1 and 2, respectively).

The dissociation products of this step are completely different, in contrast to what has been seen for the first step. In order to simplify the nomenclature, these fragments are referred to hereafter as chloroethylene-type species (monoCl).

The C–C bond lengths, calculated for both cases, are very similar to the C=C bond value in the gas-phase (see d(1–2) entry in Tables 1 and 2). This indicates that both carbon atoms still have a sp^2 hybridization.

In Scheme 1, one may note that there are two different forms for the monoCl fragment: monoCl(1)a and monoCl(1). The main difference is that in the second configuration, the fragment is completely tilted toward the surface and thus has an extra interaction with two Cu atoms. It was not possible to identify the transition state that links both species. This transformation does not refer to a dissociative process, as in the previous cases; thus the activation barrier is expected to be very low and the Ts optimization difficult. This molecular displacement is originated from a steric constraint with the Cl(3) atom (see Scheme 1). One may note that the chlorine atom (3) returns to its usual bridge position on the PdCu row in the monoCl(1) configuration.

The configuration monoCl(2) (see Scheme 2) stands up off the surface. This seems to occur because both chlorine atoms have left from the same carbon atom, which is now bond to the surface. Only one structure for this fragment has been found.

The dissociation path, which is shown in Scheme 1 up to the second C–Cl bond dissociation, can be used as a model for the dissociation reaction of *cis*-dichloroethene. For instance, Yang *et al.* (14) and Laroze (23) observed that *cis*-dichloroethene generated acetylene and a small amount of benzene on adsorption on Cu(100) and Cu(110), respectively. On coadsorbed chlorine, this dissociation yielded much less benzene (14). This experimental finding can be explained by the results presented here, replacing the Cl(4) with a H atom and following Scheme 1. A similar structure to monoCl(1) may be the precursor for the formation of acetylene and benzene, since it is already an acetylene molecule and both carbon atoms are activated for the trimerization reaction.

In a similar way the reaction path that is shown in Scheme 2 can be used as a model for the dissociation reaction of 1,1 dichloroethene. Experimentally, Laroze (23) has indicated that the main product of this reaction on Cu(110) is 1,3-butadiene. The precursor of butadiene, possibly, is an intermediate with a spatial configuration similar to monoCl(2), which stands up off the surface. The coupling of two molecules of this precursor will proceed by the carbon(2) (see Scheme 2), which is activated by the surface, to form a 4 carbon backbone fragment. A subsequent molecular coupling is not possible, since the terminal carbon atoms are not activated; thus the new fragment is hydrogenated, producing butadiene.

Trans-dichloroethene has been shown to produce acetylene on Pd(110) (1), Cu(110) (12), and PdCu(110) (39), behavior which is similar to that of the *cis*-isomer. Although none of the reaction paths studied here can be used as a model for this molecule dissociation, it is possible to propose that the precursor of acetylene should also have a flat spatial configuration, parallel to the surface, similar to the case of the *cis*-isomer.

Third Dissociation Step

The final C–Cl bond dissociation shows two different pathways. In the case of the monoCl(1), as for all steps before, this dissociation is promoted by a Cu atom, forming a Cu–Cl bond. In the case of monoCl(2) fragment it involves a Pd atom (see Schemes 1 and 2).

The activation energy for the first case (monoCl(1)) is much lower than for the case of monoCl(2): 4 and 43 kJ mol^{-1}, respectively. It is interesting to note that experimentally the activation of the C–Cl bond of CH_3CHCl_2 on Pd(111) was also found to be high (70 kJ mol^{-1}) (6).

One may observe that in the Pd case, the C–Cl bond is not activated, as it has a small elongation compared to the C–Cl bond length of the trichloroethene molecule in the gas-phase (1.72 Å) (see entry d(1–5) in Table 2). On the other hand, this bond has been already stretched about 0.08 Å in the case of the monoCl(1) fragment (see entry d(2–4) in Table 1). It is interesting that the distance between the Cl atom and the surface atom has the same value in both cases, 2.85 Å (see entries d(4–11) and d(5–6) in Tables 1 and 2, respectively). The main difference that appears in the activation energy seems to be due to the activation of the carbon atom. In the monoCl(1) case, the carbon atom interacts directly with the surface atoms, whereas in the other case the carbon atom does not.

The final product in both mechanisms is a carbon–carbon–hydrogen species (CCH), which seems to have a similar configuration but in different spatial arrangement. The chlorine atoms, which are placed around the fragment on the surface, may be responsible for this distinct spatial position. The CCH(1) species has more empty space to lay on the surface, with less steric hindrance from the chlorine atoms, whereas the CCH(2) species promotes a strong reconstruction of the surface in order to find a stable configuration (see Scheme 2). This reconstruction causes the CCH(2) species to be 36 kJ mol^{-1} less stable than the CCH(1) one (24).

4. DISCUSSION

Understanding the Bond Activation in the Transition State

As shown in the previous section, the C–Cl bond length is already elongated from its gas-phase value in most of the chemisorbed and intermediate states (see Tables 1 and 2). Hence the C–Cl bond is activated on chemisorption. In the transition states this bond is further stretched, but the resulting elongation remains moderate, from 0.13 to 0.37% of each initial state (chemisorbed or dechlorinated), which indicates an early transition state. This is often the case of strongly exothermic reactions, but contrasts with the C–H dissociation reaction on metal surfaces, where a late transition state with a strong elongated bond was found (40). In addition to the changes in the C–Cl distance, there is a global deformation of the molecule in the TS configuration, which can be related to the distortion energy of the transition state ($E_{\text{distortion}}$). This energy indicates how modified the transition-state geometry is in relation to the initial state and is calculated using the following expression:

$$E_{\text{distortion}} = E_{\text{transition-state}} - E_{\text{reactant}}. \qquad [3]$$

$E_{\text{transition-state}}$ and E_{reactant} are the energies of the molecule in the Ts and the ground-state geometries calculated far from the surface (gas-phase). Plotting the activation energy for the C–Cl dissociation against $E_{\text{distortion}}$ for the six elementary steps (see Fig. 3a), one may note the activation energy increases with the distortion energy. Hence the lowest activation energy corresponds to the earliest or least modified Ts geometry.

A good linear correlation is, however, only observed if the point that corresponds to the monoCl(2) dissociation is taken out of the linear fitting. This point is marked by

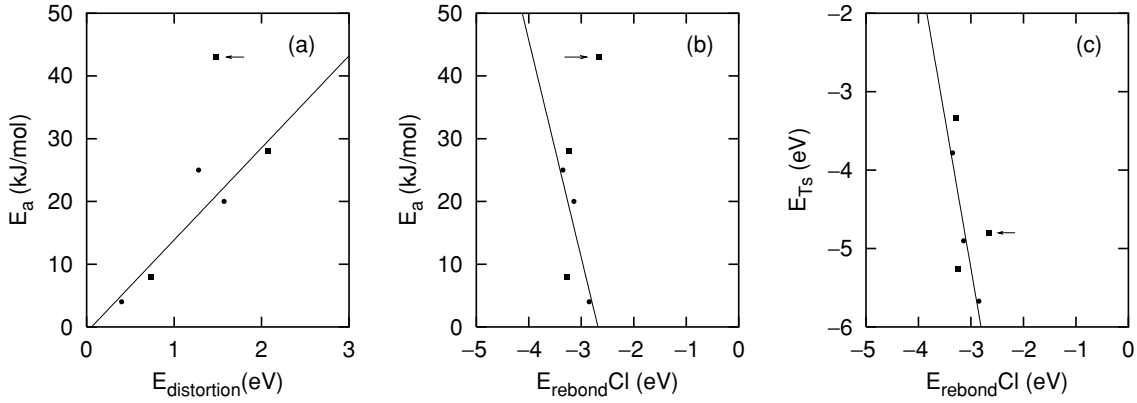

FIG. 3. Analysis of the transition state energies for the dechlorination steps. ●, Transition states results of mechanism 1; ■, transition states results of mechanism 2. (a) The activation energy (E_a) versus the distortion energy ($E_{distrotion}$) of the molecule in the Ts (see text). (b) E_a versus the rebonding energy of the Cl fragment (E_{rebond}Cl) (see text). (c) The binding energy of the transition states of all intermediary steps (E_{Ts}) versus the rebonding energy of the chlorine fragment (E_{rebond}Cl) (see text).

an arrow in Fig. 3. As indicated previously, this C–Cl dissociation is different from the other ones, since the bond is broken at a Pd atom, whereas for all the others the Cu atom is involved.

Another interesting approach to the study of transition states has been suggested by Hammer (41): the rebonding energy (E_{rebond}). This energy characterizes the extra molecular–surface bond, formed during the Ts, compared to the initial state. This approach is very useful for studying late transition states, where the molecule is almost completely dissociated. In this case, the energy of the Ts is related to the new bonds formed between the fragments and the surface. Would it be possible to apply a similar strategy in the present case?

The transition states studied by Hammer were related to the same fragments. This is not the case here, where for each transition state of the successive dissociation a different carbon–carbon fragment is formed. However, the chlorine atom is a common fragment in all transition states (see Schemes 1 and 2). Therefore, the analysis will be done in relation to the Cl fragment.

The rebonding energy of the chlorine fragments in the Ts (E_{rebond}Cl) is calculated by considering the binding energy of an isolated Cl atom to the geometry found in the TS configuration:

$$E_{rebond}\mathrm{Cl} = E^{Ts}_{Cl+surf} - E_{surf} - E_{Cl}. \qquad [4]$$

E_{surf} is the energy of the surface, calculated with the same configuration found in the Ts. In the case of Ts2 and Ts3, the E_{surf} is the energy of the surface with the chlorine atoms resulting from the previous dissociation reactions. The E_{Cl}, the energy of the chlorine fragment in gas-phase, is calculated in a similar way to E_{surf}. In all cases the unit-cell dimensions were maintained unchanged and equal to the original one.

By evaluating also the binding energy of the molecule in the transition state configuration (E_{Ts}), similarly to the E_{rebond}Cl, two new correlations can be studied; the activation energy, E_a, and the Ts binding energy, E_{Ts}, against E_{rebond}Cl (see Figs. 3b and 3c). Following the same procedure used in the previous correlation (Fig. 3a), the point that corresponds to the monoCl(2) was taken out from the linear fitting. The remaining points are, thus, related to the binding of the chlorine fragment to the Cu atom of the surface. One may note that a reasonable linear correlation has been found in both new correlations.

The low activation energy barrier is associated with low Cl rebonding energy (see Fig. 3b). This relation shows an opposite correlation from what has been seen for the similar plot constructed for the NO dissociation on Rh, Pd, and Pd_3Mn (110) surfaces (42), where the low reaction barriers were related to large binding energies. This result was indeed expected, since the NO dissociation transition state is a late one, which means that the geometry of the transition state is very similar to the geometry of the products. In the case of early Ts, the lowest barrier corresponds to the least distorted geometry for the molecule, with only very weak new bonds formed with the surface.

In Fig. 3c, E_{Ts} decreases with the increasing of E_{rebond}Cl. This means that the transition state becomes destabilized if the Cl fragment forms a strong bond with the surface. From Fig. 3a, it has been demonstrated that the lowest activation energy corresponds to the least distorted C–Cl bond; in consequence the chlorine fragment has to be weakly bond to the surface, in complete agreement with results in Figs. 3b and 3c.

Following the Dechlorination Kinetics

The transition state theory allows the calculation of the kinetic constants in terms of the local properties of the

TABLE 3

Calculated Kinetic Constants at 250 K for All Reaction Steps[a]

Mechanism[b]	Kinetic constant (k_{diss})
First dissociation	
1 (CHCl)	6.4×10^8
2 (CCl_2)	4.1×10^{11}
Second dissociation	
1 (CCl_2)	1.8×10^{10}
2 (CCl)	1.7×10^9
Third dissociation	
1 (CCl)	3.7×10^{12}
2 (CHCl)	3.7×10^5

[a] Values in s^{-1}.

[b] Number n corresponds to the reaction scheme n. The parentheses show the functional group which the dissociated C–Cl bond belongs to.

potential surface of the system. As shown in Methods, the preexponential factor can be evaluated from the vibrational partition functions and the exponential term from the calculated activation energy.

The kinetic constants for the different steps of the TCE dechlorination reaction are shown in Table 3. All values reported here are related to 250 K. At this temperature, several intermediate species (di-σ, mono- and dichloro, and CCH) of the TCE dissociation on the PdCu surface have been observed in HREELS experiments and confirmed by the calculated vibrational frequencies of optimized configurations of the dechlorinated molecules (24).

One may note that all the steps are fast and that the kinetic constant for the C–Cl bond dissociation (k_{diss}) of the CCl_2 group is more than 500 times larger than that of the CHCl group, for the first step of the TCE dechlorination reaction. This same trend is observed in the case of the second dissociation step; however the k_{diss} of the CCl_2 group is only 20 times larger in this case. Both results confirm that C–Cl bond dissociation is more favorable from the CCl_2 group.

The values of the kinetic constants indicate that each reaction path has a different limiting step (see Schemes 1 and 2); thus, one may expect that several adsorbed species will be present simultaneously on the surface during the dissociation reaction.

In order to illustrate this, a simple kinetic model of the TCE dechlorination is built up, using some approximations:

- All steps were considered irreversible, since all reactions steps in both mechanisms are highly exothermic.
- It was assumed that the reactions occur at constant temperature (250 K).
- Both dechlorination reaction mechanisms were independent, which means that the two di-σ species are considered distinct precursors of the reaction. Although these species are just different adsorption forms of the same reactant (TCE), both the geometry and adsorption energy values of the adsorption modes are distinct for each case.
- The reactants were taken as adsorbed species and not in gas-phase. Moreover, the intermediate species are not present on the surface at the beginning of the reaction.

With these assumptions, two independent differential equation systems can be formulated as

$$\frac{d[\text{di-}\sigma(i)]}{dt} = -k_{\text{diss}(1)}[\text{di-}\sigma(i)], \quad [5]$$

$$\frac{d[\text{diCl}(i)]}{dt} = +k_{\text{diss}(1)}[\text{di-}\sigma(i)] - k_{\text{diss}(2)}[\text{diCl}(i)], \quad [6]$$

$$\frac{d[\text{monoCl}(i)]}{dt} = +k_{\text{diss}(2)}[\text{diCl}(i)] - k_{\text{diss}(3)}[\text{monoCl}(i)], \quad [7]$$

$$\frac{d[\text{CCH}(i)]}{dt} = +k_{\text{diss}(3)}[\text{monoCl}(i)], \quad [8]$$

where i indicates the associated mechanism.

In order to calculate the ratio between the di-$\sigma(1)$ and di-$\sigma(2)$ species on the surface, an equilibrium was assumed between these two adsorption modes in most circumstances; thus, the residence time of each molecule on the adsorption site can be estimated using (43)

$$\tau = \tau_0 \exp\left(\frac{\Delta H_{\text{abs}}}{RT}\right). \quad [9]$$

The surface concentration σ will depend on this residence time τ and on the flux of molecules F striking the surface:

$$\sigma = \tau F. \quad [10]$$

Combining these two equations and taking into account the fact that the flux F is the same, the coverage ratio between the two different adsorption modes is equal to

$$\frac{\sigma_{\text{di-}\sigma(1)}}{\sigma_{\text{di-}\sigma(2)}} = \exp\left(\frac{\Delta H_{\text{di-}\sigma(1)} - \Delta H_{\text{di-}\sigma(2)}}{RT}\right). \quad [11]$$

Thus, knowing that the adsorption energy difference between both species is 6 kJ mol^{-1}, the surface concentration ratio is then calculated and shown to be about 20.

Having set the initial conditions for the di-σ species from the latter relation, the two differential equation systems can be evaluated, as shown in Figs. 4a and b.

The first point to be observed is that a large number of species can be present on the surface at 250 K, in very good agreement with the related HREELS experiments of the TCE dissociation on the PdCu surface (24).

The di-$\sigma(2)$ species disappears promptly (Fig. 4a). Two factors contribute to this: its low surface concentration and its fast dissociation rate. In consequence, the diCl(2) species is readily available on the surface. As the dechlorination

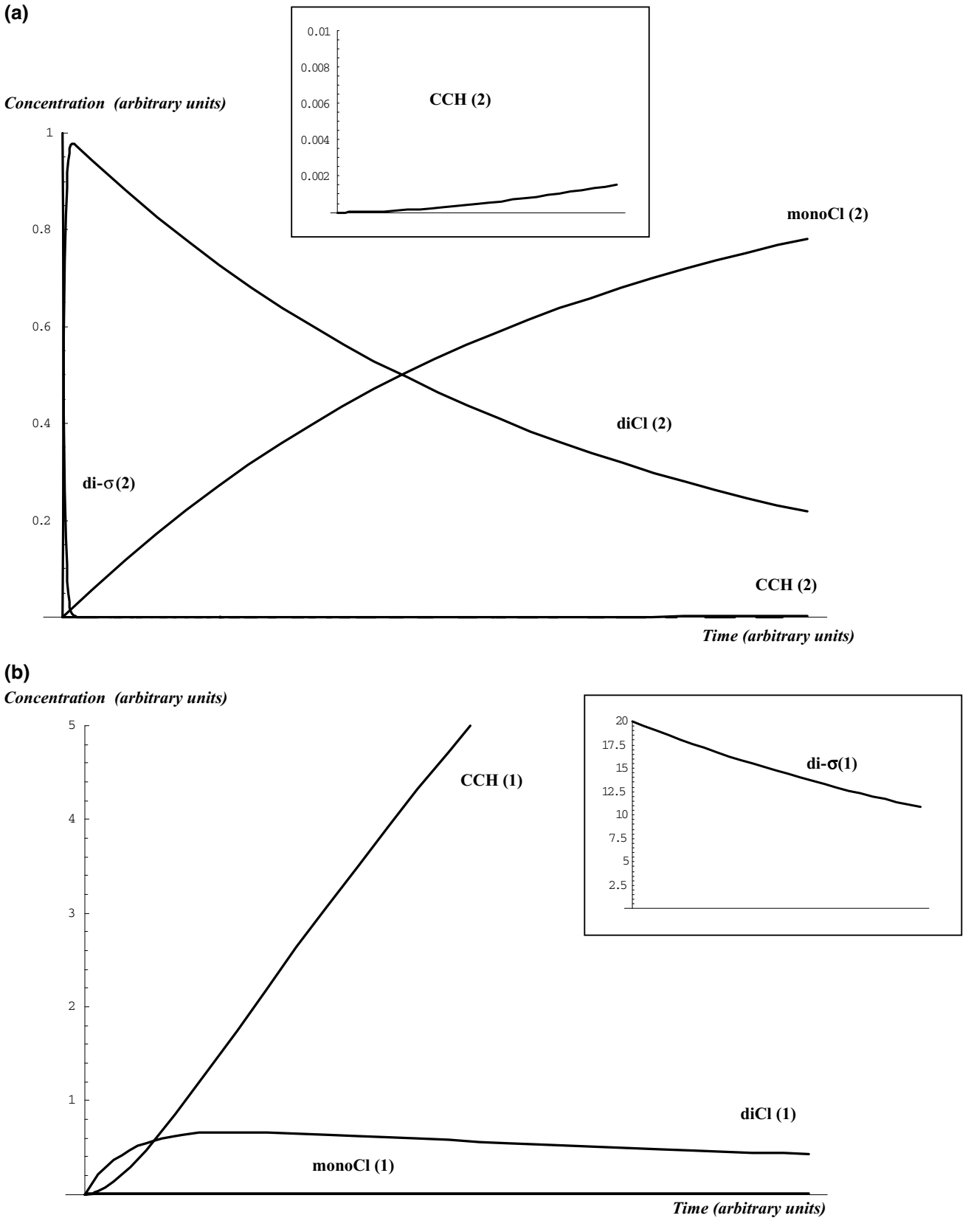

FIG. 4. Simulated concentration profile of different intermediate species on the PdCu surface with time. All graphs have the same time scale. (a) Dechlorination reaction with the di-$\sigma(2)$ precursor. (b) Dechlorination reaction with the di-$\sigma(1)$ precursor.

reaction proceeds, the monoCl(2) species accumulates on the surface due to its low dissociation rate. The final product (CCH(2)) is also present but at very low concentration.

In Fig. 4b, the trend is complete different. The concentration of the two chlorinated intermediates (diCl(1) and monoCl(1)) is very small, due to their fast dissociation rate (see the kinetic constants in Table 3). It is interesting that the first dissociation is the limiting step in this case, in good agreement with several experimental studies (6, 10, 13).

Experimentally, the main product, which is formed in the dechlorination of TCE on Cu(110) (9) and in its hydrochlorination on Pd(110) (44), is acetylene. In the latter case, there are two other reaction products: ethene and 1,1-dichloroethene. Although the presence of hydrogen on the surface has been not studied here and it may induce different reaction channels, the precursors of these three products can be suggested. For the case of both ethene and acetylene this species is the CCH(1) fragment, because it is readily available on the surface (Fig. 4b) and can be hydrogenated promptly; note that the CCH(1) species interacts with two Pd atoms (Scheme 1).

For the case of the dichloroethene production there are two possible surface precursors: diCl(2) and diCl(1) species. Although the diCl(2) formation is the fastest one (Fig. 4a), the concentration of this species and its hydrogenation product (*trans*-dichloroethene) on the surface is negligible, due to the very small initial concentration of the chemisorbed di-σ(2) species.

The diCl(1), product of the di-σ(1) species dissociation, is present on the surface with similar concentration to diCl(2). However, this concentration decreases slowly due to two factors: the large concentration of di-σ(1) species and the similar dissociation rate between the first and second reaction steps (see Fig. 4b and Table 3). Therefore, the hydrogenated product (1, 1-dichloroethene) is formed continuously. Moreover, this is in agreement with the suggestion of CCH(1) being the precursor of acetylene and ethene formation.

5. CONCLUSIONS

In the present work the dissociation of the trichloroethene on the PdCu(110) surface has been investigated systematically. This study involves a model system, in clear relation to surface science experiments. Although in a real catalytic condition the reaction system could be more complex (alloy surface composition and structure changes, surface carbiding, and presence of hydrogen), some insights into the transition states and the reaction steps of this dissociation have been proposed by applying *ab initio* periodic density functional theory.

Two different mechanisms have been studied, starting from the most stable adsorption modes of trichloroethene (di-σ structures). Regarding the different pathways, all intermediary steps of the reaction are exothermic. In addition, all activation energies are relatively small (<40 kJ mol^{-1}). Therefore, the dechlorination reaction is shown to be kinetically and thermodynamically favorable on this surface.

Also from the study of these mechanisms, it was possible to attain additional information about the dechlorination reaction of other chloroethene molecules (dichloro and chloro). There is a good evidence that the intermediates and transition states of these chloroethene dissociations have a similar configuration on the PdCu(110) surface.

Regarding the study of the transition states of the intermediary steps, a low activation energy of the dissociation step is associated with a weakly distorted molecule in the transition state. This is related to the early nature of the Ts.

A simple kinetic model, constructed with the calculated rate constants, allows the understanding of the complex dissociation reaction of TCE. Several intermediates of the reaction are present simultaneously on the surface, in accordance with experimental studies.

ACKNOWLEDGMENTS

The authors thank Prof. Rasmita Raval, Dr. Yvette Jugnet, and Prof. Jean-Claude Bertolini for useful discussions, and IDRIS at CNRS for the attribution of CPU time under project no. 609. This project was possible due to the European Associated Laboratory between the Leverhulme Centre for Innovative Catalysis and the Institut de Recherches sur la Catalyse.

REFERENCES

1. Bloxham, L. H., Haq, S., Mitchell, C., and Raval, R., *Surf. Sci.* **489**, 1 (2001).
2. Jenks, C. J., Bent, B. E., Bernstein, N., and Zaera, F., *J. Phys. Chem.* B **104**, 3008 (2000).
3. Lowry, G. V., and Reinhard, M., *Environ. Sci. Technol.* **34**, 3217 (2000).
4. Benitez, J. L., and del Angel, G., *React. Kinet. Catal. Lett.* **70**, 67 (2000).
5. Cabibil, H., Ihm, H., and White, J. M., *Surf. Sci.* **447**, 91 (2000).
6. Zhou, G., Chan, C., and Gellman, A. J., *J. Phys. Chem.* B **103**, 1134 (1999).
7. Buelow, M. T., Zhou, G., Gellman, A. J., and Immaraporn, B., *Catal. Lett.* **59**, 9 (1999).
8. Chan, A. S. Y., Turton, S., and Jones, R. G., *Surf. Sci.* **433–435**, 234 (1999).
9. Laroze, S. C., Haq, S., Raval, R., Jugnet, Y., and Bertolini, J. C., *Surf. Sci.* **433–435**, 193 (1999).
10. Chan, C., and Gellman, A. J., *Catal. Lett.* **53**, 139 (1998).
11. Rochefort, A., Martel, R., and McBreen, P. H., *Surf. Sci.* **414**, 38 (1998).
12. Jugnet, Y., Prakash, N. S., Bertolini, J. C., Laroze, S. C., and Raval, R., *Catal. Lett.* **56**, 17 (1998).
13. Yang, M. X., Sarkar, S., Bent, B. E., Bare, S. R., and Holbrook, M. T., *Langmuir* **13**, 229 (1997).
14. Yang, M. X., Kash, P. W., Sun, D.-H., Flynn, G. W., Bent, B., Holbrook, M. T., Bare, S. R., Fischer, D. A., and Gland, J. L., *Surf. Sci.* **380**, 151 (1997).
15. Karpinski, Z., Early, K., and d'Itri, J. L., *J. Catal.* **164**, 378 (1996).
16. Yang, M. X., Eng Jr., J., Kash, P. W., Flynn, G. W., Bent, B., Holbrook, M. T., Bare, S. R., Gland, J. L., and Fischer, D. A., *J. Phys. Chem.* **100**, 12431 (1996).

17. Cassuto, A., Hugenschmidt, M. B., Parent, Ph., Laffon, C., and Tourillon, H. G., *Surf. Sci.* **310**, 390 (1994).
18. Lin, J.-L., and Bent, B. E., *J. Phys. Chem.* **97**, 9713 (1993).
19. Lin, J.-L., and Bent, B. E., *J. Phys. Chem.* **96**, 8529 (1992).
20. Ohnishi, R., Wang, W.-L., and Ichikawa, M., *Appl. Catal. A* **113**, 29 (1994).
21. Thompson, C. D., Rioux, R. M., Chen, N., and Ribeiro, F. H., *J. Phys. Chem. B* **104**, 3067 (2000).
22. Rioux, R. M., Thompson, C. D., Chen, N., and Ribeiro, F. H., *Catal. Today* **62**, 269 (2000).
23. Laroze, S. C., Ph.D. thesis. University of Liverpool, England, 1999.
24. Jugnet, Y., Bertolini, J.-C., Barbosa, L. A. M. M., and Sautet, P., *Surf. Sci.*, in press.
25. Kresse, G., and Furthmüller, J., *Comp. Mater. Sci.* **6**, 15 (1996).
26. Kresse, G., and Furthmüller, J., *Phys. Rev. B* **54**, 169 (1996).
27. Perdew, J., and Zunger, A., *Phys. Rev. B* **23**, 8054 (1981).
28. Perdew, J., and Wang, Y., *Phys. Rev. B* **33**, 8800 (1986).
29. Vanderbilt, D., *Phys. Rev. B* **41**, 7892 (1990).
30. Kresse, G., and Hafner, J., *J. Phys. Condens. Matter* **6**, 8245 (1994).
31. Lianos, L., Debauge, Y., Massardier, J., Jugnet, Y., and Bertolini, J.-C., *Catal. Lett.* **44**, 211 (1997).
32. Barbosa, L. A. M. M., Loffreda, D., and Sautet, P., *Langmuir*, in press.
33. Villar, A. P., and Calvet, L. D., "Pearson's Handbook of Crystallography Data for Intermetallic Phases," ASM International, Materials Park, OH, 1991.
34. Schlegel, H. B., *in* "AB initio Methods in Quantum Chemistry—I" (K. P. Lawley, Ed.), p. 249. Wiley, New York, 1987.
35. van Santen, R. A., and Niemanstsverdriet, J. W., *in* "Chemical Kinetics and Catalysis" (M. V. Twigg and M. S. Spencer, Eds.), p. 105. Plenum, New York, 1995.
36. Loffreda, D., Simon, D., and Sautet, P., *Chem. Phys. Lett.* **291**, 15 (1998).
37. Loffreda, D., Simon, D., and Sautet, P., *Surf. Sci.* **425**, 68 (1999).
38. Delbecq, F., and Sautet, P., *Surf. Sci.* **442**, 338 (1999).
39. Bloxham, L. H., Haq, S., Jugnet, Y., Bertolini, J.-C., and Raval, R., in preparation.
40. Sebastian, J., Ph.D. thesis. Ecole Normale Supérieure de Lyon, France, 2001.
41. Hammer, B., *Surf. Sci.* **459**, 323 (2000).
42. Loffreda, D., Delbecq, F., Simon, D., and Sautet, P., *J. Chem. Phys.* **115**, 8101 (2001).
43. Somorjai, G. A., "Introduction to Surface Science and Catalysis." Wiley, New York, 1994.
44. Jugnet, Y., and Bertolini, J.-C., to be published.